Lyle, M., Koizumi, I., Richter, C., and Moore, T.C., Jr. (Eds.), 2000
Proceedings of the Ocean Drilling Program, Scientific Results, Vol. 167

18. LATE PLEISTOCENE RECORD OF TERRIGENOUS MINERAL DEPOSITION ALONG THE NORTHERN CALIFORNIA MARGIN (SITES 1018 AND 1020)[1]

S.A. Hovan,[2] S.W. Kish,[2] and H.J. Renyck[2]

ABSTRACT

The terrigenous mineral fraction of sediments recovered by drilling during Ocean Drilling Program Leg 167 at Sites 1018 and 1020 is used to evaluate changes in the source and transport of fine-grained terrigenous sediment and its relation to regional climates and the paleoceanographic evolution of the California Current system during the late Pleistocene. Preliminary time scales developed by correlation of oxygen isotope stratigraphies with the global SPECMAP record show average linear sedimentation rates in excess of 100 m/m.y., which provide an opportunity for high-resolution studies of terrigenous flux, grain size, and mineralogy. The mass flux of terrigenous minerals at Site 1018 varies from 5 to 30 $g(cm^2 \cdot k.y.)^{-1}$ and displays a general trend toward increased flux during glacials. The terrigenous record at Site 1020 shows a similar pattern of increased glacial input, but overall accumulation rates are significantly lower. Spectral analysis demonstrates that most of this variability is concentrated in frequency bands related to orbital cycles of eccentricity, tilt, and precession. Detailed grain-size analysis performed on the isolated terrigenous mineral fraction shows that sediments from Site 1018 are associated with higher energy transport and depositional regimes than those found at Site 1020. Grain-size data are remarkably uniform throughout the last 500 k.y., with no discernible difference observed between glacial and interglacial size distributions within each site. X-ray diffraction analysis of the <2-µm clay component suggests that the deposition of minerals found at Site 1020 is consistent with transport from a southern source during intervals of increased terrigenous input.

INTRODUCTION

Sediments recovered during drilling of Ocean Drilling Program (ODP) Leg 167 along the California margin reveal important information for paleoclimate and paleoceanographic studies. Because they monitor regions of very high marine primary production, they can record changes in upwelling timing and intensity, track intermediate and deep-water transport pathways, and provide evidence for linkages between continental and marine systems. Shipboard data indicate that Leg 167 sites provide continuous records with generally abundant carbonate and foraminifers available for stable isotopic determination (Shipboard Scientific Party, 1997a, 1997b). Moreover, very high sedimentation rates along the margin make these sites suitable to address questions about the evolution of the California Current system and its link to paleoclimatic conditions from millennial to orbital time scales. Standard piston cores provide very useful records, but the high rate of sedimentation makes it difficult to sample a full glacial cycle even with the longest cores available without drilling. Previous drilling along the California margin occurred during the Deep Sea Drilling Project (DSDP) before the advent of advanced hydraulic piston corer technology and recovered core that was discontinuous and very disturbed, thus unsuitable for modern, high-resolution paleoceanographic studies.

The sediments recovered during Leg 167 represent a mixture of terrigenous clays and silts, biogenic silica, and carbonate. Each of these components can be helpful in deciphering the paleoclimatic history of this region; however, this study will focus on the input of terrigenous material at two sites along the northern California margin, ODP Sites 1018 and 1020. The input of terrigenous sediment carries with it important information about climatic conditions on the continent and about mechanisms and/or processes by which the material is transported to the site of deposition. The amount or mass flux of terrigenous minerals reflects the supply of sediment in the continental source region and can provide an important signal of changes related to precipitation and climate (Griggs and Hein, 1980; Karlin, 1980; Griggs, 1987). Likewise, the grain size of terrigenous mineral material can be used to characterize the process and intensity of transport. Ledbetter (1986) showed the distinct influence abyssal currents have on terrigenous component grain size for the southwest Atlantic. Dowling and McCave (1993) identified changes in bottom current activity since the last glacial maximum based upon the varying importance of size modes in detrital silt along the Fenni Drift. Others used grain-size distributions to discern different transport and depositional processes and assist in the paleoenvironmental interpretation of terrigenous signals (Rea and Hovan, 1995; Joseph et al., 1998; Boven and Rea, 1998).

The provenance and relative importance of continental source regions can be traced by the regional pattern of terrigenous clay mineralogy (Karlin, 1980; Krissek, 1982; Petschick et al., 1996). In the northeast Pacific, Karlin (1980) found that modern terrigenous sediments deposited along the continental margin were supplied by two main sources: (1) a chlorite- and illite-rich source input by streams of the northern California Coastal Range and Klamath Mountains, and (2) a smectite-rich (montmorillonite) component from discharge of the Columbia River Basin. Clay mineral distribution patterns also record dominant dispersal pathways in this region and are strongly influenced by coastal currents (Karlin, 1980; Krissek, 1982). Thus, with the high-resolution records of terrigenous sedimentation recovered during Leg 167 and using modern surface sediment as a reference, we should be able to track changes in the late Pleistocene location of dominant current systems transporting terrigenous sediment in this region.

Here we show the results of our effort to study physical and mineralogical tracers of terrigenous sediment in an attempt to identify regional climatic controls and possible transport pathways during the past few glacial cycles of the late Pleistocene.

SITE SELECTION AND ANALYTICAL METHODS

This manuscript presents the results of our study of the terrigenous component of sediment deposited along the northern California margin—particularly Sites 1018 and 1020 (Fig. 1). Composite strati-

[1]Lyle, M., Koizumi, I., Richter, C., and Moore, T.C., Jr. (Eds.), 2000. *Proc. ODP, Sci. Results,* 167: College Station TX (Ocean Drilling Program).

[2]Geoscience Department, Indiana University of Pennsylvania, 114 Walsh Hall, Indiana PA 15705-1087, USA. Correspondence author: hovan@grove.iup.edu

graphic sections were developed for each site using high-resolution shipboard measurements of gamma-ray attenuation porosity evaluator (GRAPE), magnetic susceptibility, and color reflectance data (Lyle, Koizumi, Richter, et al., 1997). Site 1018 is located ~75 km west of Santa Cruz, California, on a sediment drift deposit just south of the Guide Seamount at a water depth of 2477 meters below sea level (mbsl). This site is on top of a sediment mound that is elevated from surrounding sediments by more then 400 m. Overall sedimentation rates are extremely high, averaging 100 to 400 m/m.y. during the late Pleistocene, reflecting the site's close proximity to its sediment source in the north from Pioneer Canyon, west of San Francisco Bay (Lyle, Koizumi, Richter, et al., 1997). Site 1018 was selected to provide a nearshore end-member of terrigenous sediment supplied from the area draining the central and northern California Coastal Range. Site 1020 contains a continuous sequence of sediment deposited at rates in excess of 100 m/m.y. during the late Pleistocene. It is located on the east flank of the Gorda Ridge on an abyssal hill at a water depth of 3038 mbsl. To the east of Site 1020, the floor of the Gorda Basin is covered with thick Pleistocene turbidite deposits, but the site itself contains only a few, thin turbidite layers (these intervals were avoided during sampling). Site 1020 is located between major sources of sediment supplied from the Columbia River to the north and the Klamath, Eel, and Rogue Rivers to the south. This site should enable us to evaluate the relative importance and magnitude of various continental sources and provide a deeper water, offshore signal of terrigenous input.

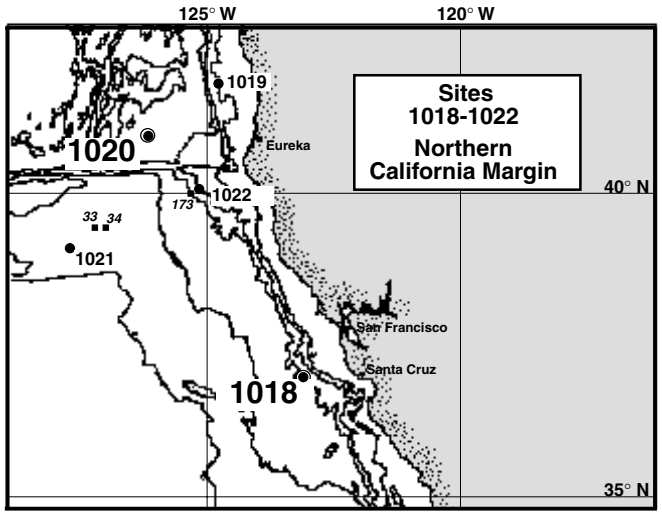

Figure 1. Location map of Sites 1018 and 1020 along the northern California margin.

The terrigenous mineral fraction of these samples was isolated using a series of chemical leaches that sequentially dissolves biogenic and authigenic phases. Carbonates were removed by treating each sample with a weak acetic acid solution. A buffered sodium citrate and sodium hydrosulfite solution was used to remove oxides, hydroxides, and zeolites, and warm sodium carbonate baths were used to dissolve biogenic silica. Details of this procedure were provided by Rea and Janecek (1981). The resulting precision of this method determined from duplicate analyses is ~±5% relative error. Note that this method provides a segregated sample of terrigenous material that can be analyzed further for physical, chemical, and mineralogical parameters without concern about the dilution or contamination that often accompanies analysis of bulk sediment or other proxy measures of the terrigenous component.

The mass flux or mass accumulation rate (MAR) of terrigenous material was determined by the product of the linear sedimentation rate (LSR), dry bulk density (DBD), and weight percentage of terrigenous material for each sample as follows:

$$\text{terrigenous MAR } (\text{g}[\text{cm}^2 \cdot \text{k.y.}]^{-1}) = \\ \%\ \text{extracted} \times \text{LSR } (\text{cm} \cdot \text{k.y.}^{-1}) \times \text{DBD } (\text{g} \cdot \text{cm}^{-3}).$$

Dry bulk densities were determined from shipboard GRAPE measurements using the relationship given by Boyce (1976). Linear sedimentation rates were calculated from age models constructed by correlation of the foraminiferal oxygen isotope stratigraphy at each site (see Lyle et al., Chap. 11, this volume) with the SPECMAP global chronology (Imbrie et al., 1984). At the time of publication, only preliminary oxygen isotopic correlation age models were available for these sites. The record from Site 1018 was complete through Stage 6 (186 ka) and from Site 1020 through Stage 9 (339 ka), beyond which we extrapolated age and linear sedimentation rate data between two control points provided by the top of *Pseudoemiliania lacunosa* datum (460 ka) and the Brunhes magnetostratigraphic Chron (780 ka). All data used to calculate the terrigenous MAR are provided in Tables 1 and 2 and Figure 2. Although we show terrigenous data collected beyond ages in the oxygen isotope age model, we have excluded these from our discussion and interpretation until we are more confident in our age assignments.

Detailed grain-size measurements of the isolated terrigenous component were made using an electronic particle size analyzer (Coulter Counter multisizer). This device measures the spherical volume equivalent of each particle counted as it is drawn through an electrical field. Mean grain size and standard deviation (sorting) data were calculated for each sample from a total size distribution based on a count of 150,000 particles divided into 256 size channels in the range of 1–30 µm. Precision of data is generally within ±0.5 µm based on replicate analyses.

Table 1. Data used to calculate the mass accumulation rate of terrigenous material and grain-size variations in sediments from Site 1018.

Hole	Core	Section	Top (cm)	Bottom (cm)	Depth (mbsf)	Depth (mcd)	Age (ka)	LSR (cm · k.y.$^{-1}$)	DBD (g · cm^{-3})	%Terr.	Terr. MAR (g[cm^2 · k.y.]$^{-1}$)	Size (µm)	Sorting (µm)
1018C	1H	1	15	18	0.17	0.09	1.3	17.54	0.65	38.46	4.37		
1018C	1H	1	55	58	0.57	0.49	3.6	17.65	0.65	62.53	7.15	4.63	8.73
1018C	1H	1	75	78	0.77	0.69	4.7	17.70	0.65	51.04	5.85		
1018C	1H	1	115	118	1.17	1.09	7.0	17.61	0.68	62.00	7.45	4.97	8.98
1018C	1H	1	135	138	1.37	1.29	8.1	17.74	0.67	67.60	7.98		
1018C	1H	2	17	20	1.69	1.61	9.9	17.70	0.75	65.37	8.70	3.49	6.41
1018C	1H	2	45	48	1.97	1.89	10.9	64.71	0.72	66.79	31.00		
1018C	1H	2	85	88	2.37	2.29	11.6	44.00	0.73			4.38	7.92
1018C	1H	2	105	108	2.57	2.49	12.2	23.40	0.75	70.41	12.40		
1018C	1H	2	145	148	2.97	2.89	15.6	12.64	0.77	60.90	5.93	3.97	7.36

Notes: Sorting data presented are expressed as a standard deviation of the grain-size distribution; blank spaces = unavailable or lost data. LSR = linear sedimentation rate, DBD = dry bulk density, Terr. = terrigenous, MAR = mass accumulation rate.

This is a sample of the table that appears on the volume CD-ROM.

Table 2. Data used to calculate the mass accumulation rate of terrigenous material and grain-size variations in sediments from Site 1020.

Hole	Core	Section	Top (cm)	Bottom (cm)	Depth (mbsf)	Depth (mcd)	Age (ka)	LSR (cm · k.y.$^{-1}$)	DBD (g · cm^{-3})	%Terr.	Terr. MAR (g[cm^2 · k.y.]$^{-1}$)	Size (μm)	Sorting (μm)
1020C	1H	1	15	18	0.17	0.17	1.3	12.50	0.65	58.00	4.69	2.90	5.11
1020C	1H	1	35	38	0.37	0.35	2.8	12.50	0.65	76.20	6.17	2.70	4.69
1020C	1H	1	55	58	0.57	0.57	4.5	12.50	0.72	96.50	8.65		
1020C	1H	1	75	78	0.77	0.77	6.1	12.50	0.70				
1020C	1H	1	95	98	0.97	0.97	7.7	12.50	0.67	74.50	6.19	2.57	4.34
1020C	1H	1	115	118	1.17	1.17	9.3	12.50	0.70	63.80	5.58	2.75	5.22
1020C	1H	1	135	138	1.37	1.37	10.9	12.50	0.73	77.70	7.14	2.76	4.48
1020C	1H	2	5	8	1.57	1.57	12.4	17.34	0.75	81.20	10.59		
1020C	1H	2	25	28	1.77	1.77	13.5	17.34	0.93	76.80	12.33	3.14	5.73
1020C	1H	2	45	48	1.97	1.97	14.7	17.34	0.91	75.70	11.92	3.43	6.24

Notes: Sorting data are expressed as a standard deviation of the grain-size distribution; blank spaces = unavailable or lost data. LSR = linear sedimentation rate, DBD = dry bulk density, Terr. = terrigenous, MAR = mass accumulation rate.

This is a sample of the table that appears on the volume CD-ROM.

The clay mineralogy of the terrigenous component was determined on a subset of samples using X-ray diffraction pattern analysis. Samples were centrifuged to segregate the <2-μm fraction and X-rayed from 2° to 30° 2θ at 45kV and 40 mA using the XDS Scintag 2000 X-ray diffractometer at the University of Rhode Island. Peak areas for each phase were normalized to an internal standard (10% talc) and converted to weight percentages according to the weighting factors given by Heath and Pisias (1979). The mineral phases quantified were smectite (17Å; 001, expanded by ethylene glycol), illite (10Å; 001), chlorite (7Å; 002), and kaolinite (7Å; 001). The 7Å peak is divided between kaolinite and chlorite in proportion to the relative intensities of their 3.58Å (002) and 3.54Å (004) peaks, respectively (Biscaye, 1965).

RESULTS

Terrigenous mineral input dominates the sediments found along the northern California margin, comprising an average of 70–80 wt% of the bulk sediment composition (Fig. 2). As such, there are only slight downcore variations in the dry bulk density, and linear sediment rates generally reflect changes in the amount of terrigenous mineral contribution. The overall terrigenous accumulation rate is significantly greater at Site 1018 compared to Site 1020, a difference that becomes more pronounced during glacial periods. Terrigenous MAR at Site 1018 averages 15.06 g(cm^2 · k.y.)$^{-1}$ (N = 174; σ = 9.10) but varies from 5 to 20 g(cm^2 · k.y.)$^{-1}$ throughout the late Pleistocene. At Site 1020, which is farther offshore and deeper, terrigenous mass accumulation and variability are significantly reduced, averaging about 8.81 g(cm^2 · k.y.)$^{-1}$ (N = 336; σ = 3.29). Both sites display a general trend toward increased terrigenous flux during glacial periods, although the details of this comparison vary slightly at each location. Spectral analysis confirms a strong relationship between terrigenous flux and glacial–interglacial periodicity with clear periodicity concentrated at the orbital frequencies of eccentricity, tilt, and precession (Fig. 3A, B). Cross-spectral analysis shows that the terrigenous flux records are coherent and in-phase (i.e., greater terrigenous flux during glacial $\delta^{18}O$ values) with SPECMAP at 100, 41, and 19 k.y. (Fig. 4).

Grain-size data also display important differences between Sites 1018 and 1020. Average grain-size distributions for terrigenous sediment from Site 1018 are coarser and more poorly sorted than those deposited at Site 1020 (Fig. 5). Terrigenous minerals at Site 1018 are characterized by a moderately sorted, broad size distribution centered with a mode near 4 μm that peaks at ~1 wt% (Fig. 5A). Downcore there is little variation, with mean grain-size values averaging 3.87 μm (N = 164; σ = 0.53) and sorting values (shown as standard deviation of the grain-size distribution) of 7.26 μm (σ = 0.82) during the past 300 k.y. At Site 1020, size distributions show a size mode near 3 μm that peaks at 2 wt%, are better sorted, contain a significant amount of smaller material, and are concave up in the coarse tail (Fig. 5B). They are remarkably uniform throughout the late Pleistocene, with average mean grain-size values of 2.89 μm (N = 244; σ = 0.17) and sorting values of 5.18 μm (σ = 0.49). Grain-size data vary at a higher frequency than terrigenous mass accumulation rate but show no obvious relationship to glacial cycles or orbital periodicity (Fig. 3C, D).

A subset of samples was selected for clay mineral analysis. Ideally, we wished to compare mineralogical variation at both sites; however, constraints imposed by time and instrumentation permitted only analysis of Site 1020 at the time of publication. The normalized clay mineral content varies considerably downcore (Fig. 6). In general, illite is most abundant, comprising as much as 50% of the clay fraction, but its percentage varies throughout the interval. Chlorite and smectite percentages are less variable but also less abundant, averaging ~15% and 7%, respectively. Kaolinite contributes little to the clay mineral assemblage in these sediments. The low-resolution nature of clay mineralogy data makes it difficult to identify temporal patterns; however, the data show a general increase in the input of chlorite minerals during intervals of increased terrigenous flux. Likewise, smectite shows a general inverse pattern and is reduced during these intervals. This is more clearly evident in the upper and lower portion of the record and less so during isotopic Stages 6 through 8.

INTERPRETING TERRIGENOUS RECORDS

Downcore variations in the mass input of terrigenous material provide an important signal of changes in source area climate. In modern systems, large variations occur in the amount of sediment delivered to the seafloor of the northeast Pacific that are directly linked to large flood events along coastal areas and more efficient transport of sediment at times of peak river discharge (Griggs and Hein, 1980; Griggs, 1987). On longer time scales, however, sediment yield is more closely related to sediment supply in the source area, which can vary with a combination of factors: basin relief and area, changes in sea level, and climatic factors such as precipitation or vegetative cover (Milliman and Syvitski, 1992; Rea, 1992). Within the time scale of the late Pleistocene, tectonic factors (basin relief and area) do not change significantly. The deposition of terrigenous material on the seafloor mainly reflects some combination of sediment supply from shallow shelf regions exposed during glacioeustatic sea-level changes and variations in precipitation/erosion in the source area drainage basin associated with shifts in climate.

Both Sites 1018 and 1020 show a significant increase in terrigenous accumulation rate during times of glaciation. Glacial terrigenous flux values are more than twice the values observed during interglacial episodes. Spectral and cross-spectral analysis performed on the 0–300 ka portion of these records confirms this pattern and shows that increased terrigenous flux values are coherent and in-phase with

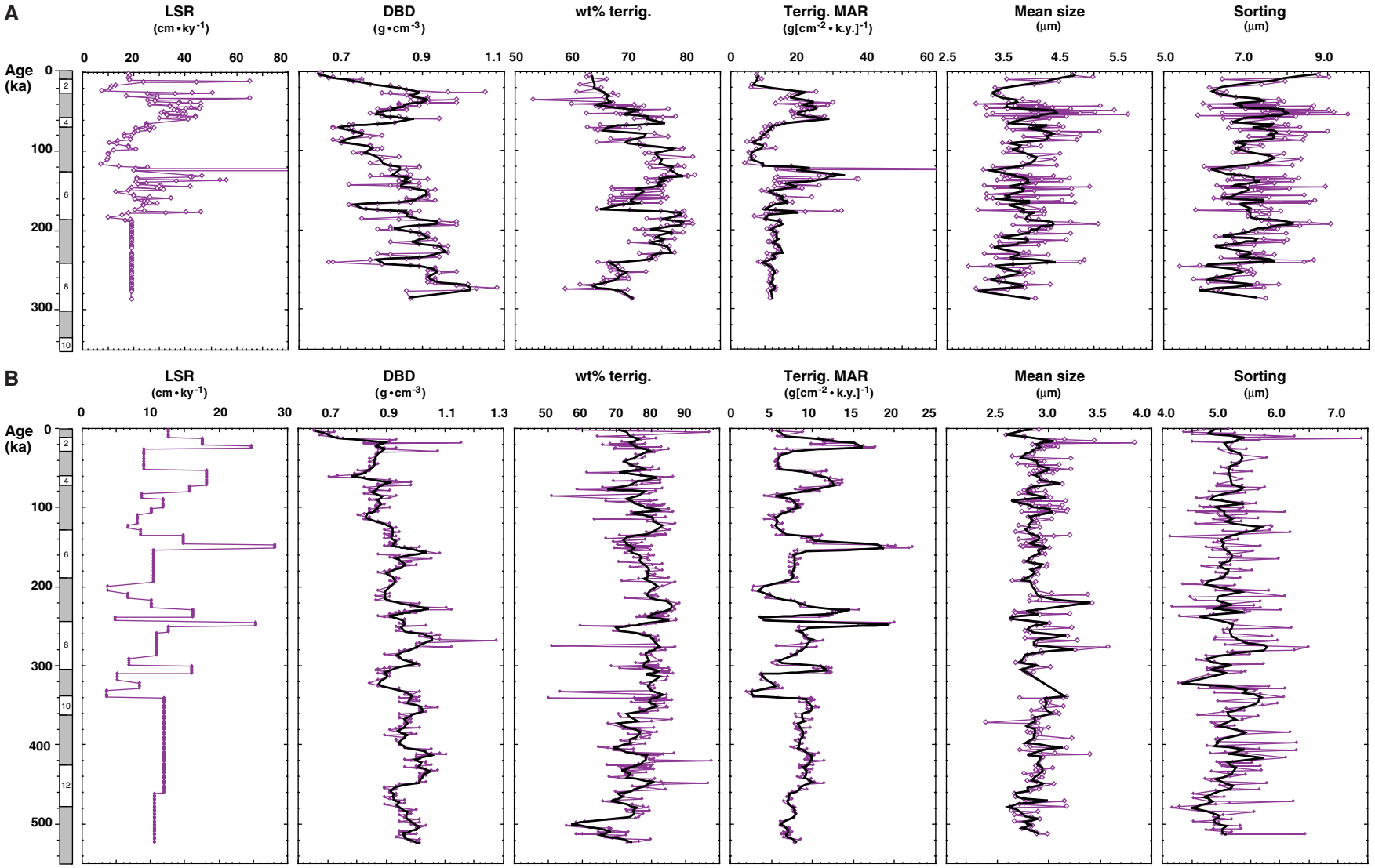

Figure 2. Temporal variations in LSR, DBD, terrigenous mineral percentage, flux, and grain size from (**A**) Site 1018 and (**B**) Site 1020. Heavy darker line indicates weighted average values. Note different data value scales used for each site. LSR = linear sedimentation rate, DBD = dry bulk density, Terrig. = terrigenous, MAR = mass accumulation rate.

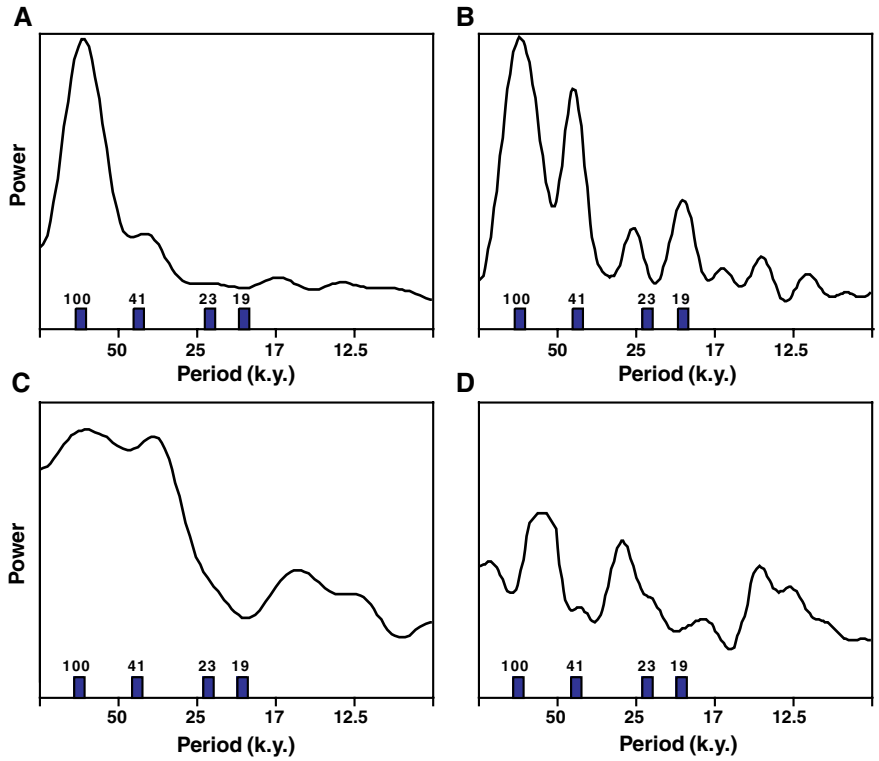

Figure 3. Power spectra calculated from the unsmoothed terrigenous flux time series for (**A**) Site 1018 and (**B**) Site 1020 shows significant variability at major orbital periodicities. Terrigenous grain-size data from (**C**) Site 1018 and (**D**) Site 1020 display much higher frequency variability and no obvious relationship to orbital cycles. Blackman-Tukey spectral analysis performed using Analyseries software package. Bandwidth is 0.009752 with a time step of 2 k.y. and 87 lags.

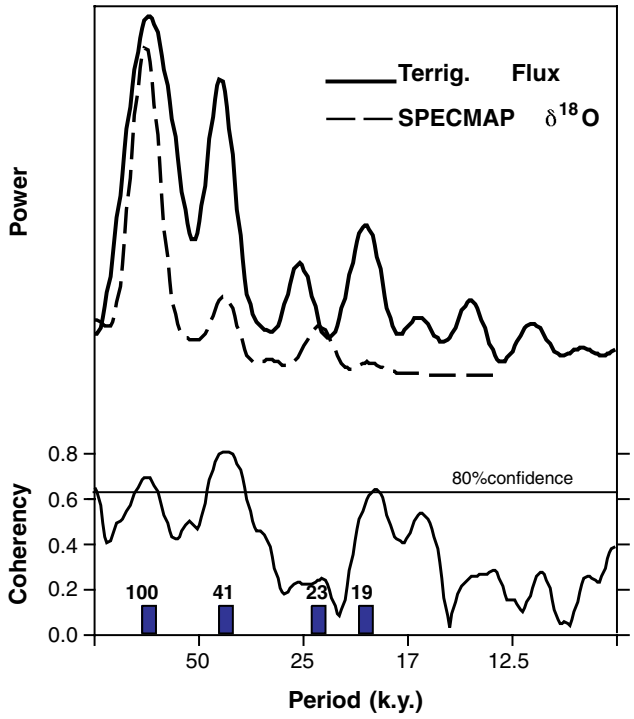

Figure 4. Cross-spectral analysis between the terrigenous flux at Site 1020 and SPECMAP $\delta^{18}O$ time series shows coherency at 100, 41, and 19 k.y.

oxygen isotopic records at each of the major Milankovitch periodicities. Implicit in this pattern is that there was an enhanced supply of terrigenous mineral grains to the northern California margin coincident with periods of glacial advance in the Northern Hemisphere. To distinguish whether this increase is related to sea-level changes or to climatic factors requires some knowledge of the provenance, transport, and depositional processes associated with these deposits.

Terrigenous mineralogy provides a reasonably good tracer of provenance in this area of the Pacific (Karlin, 1980; Krissek, 1982). Modern transport of clay minerals suggests that terrigenous material deposited at Site 1018 monitors the supply of sediment transported from sources draining Northern and Central California, whereas sediment at Site 1020 receives a mixture of material supplied from northern sources draining the Columbia River Basin and southern sources draining the Coastal Range of California and southern Oregon (Karlin, 1980). The downcore record of clay mineral abundance at Site 1020, however, shows increased illite and chlorite content during intervals of enhanced terrigenous input, suggesting that much of this material may be transported from southern source regions. Depositional records at Site 1020, therefore, probably represent a distal record of sediment supplied to Site 1018. This is not surprising given the similar temporal variability observed in terrigenous input at each location. However, to interpret whether terrigenous mass flux data record changing sea level or climatic factors requires more information about transport pathways and depositional processes.

Recent studies involving terrigenous mineral size distributions suggest that they may permit reasonably good delineation of the dominant mode of sediment transport to the seafloor (Ellwood and Ledbetter, 1977, 1979; Rea and Hovan, 1995; Joseph et al., 1998). These studies show that distinct differences exist between the size distributions associated with sediment found in hemipelagic, drift, and turbidite depositional regimes. Although a few thin turbidite layers were identified throughout the upper sections of sediments at these sites (Lyle, Koizumi, Richter, et al., 1997), grain-size distribution data suggest we were successful in avoiding them during sampling for this study. Grain-size distributions for Site 1018 are characterized by a coarser mean size broadly distributed over 1–30 µm and are more similar to sediments found in higher energy drift deposits. Size distributions for Site 1020 are finer grained with better sorting, reflecting sedimentation under lower energy hemipelagic conditions. When plotted together, the grain-size data fall along a mixing line between end-members represented by samples from each site, which indicates that sediments from Site 1020 may also represent a distal counterpart to Site 1018 with respect to transport mode and deposition process (Fig. 7).

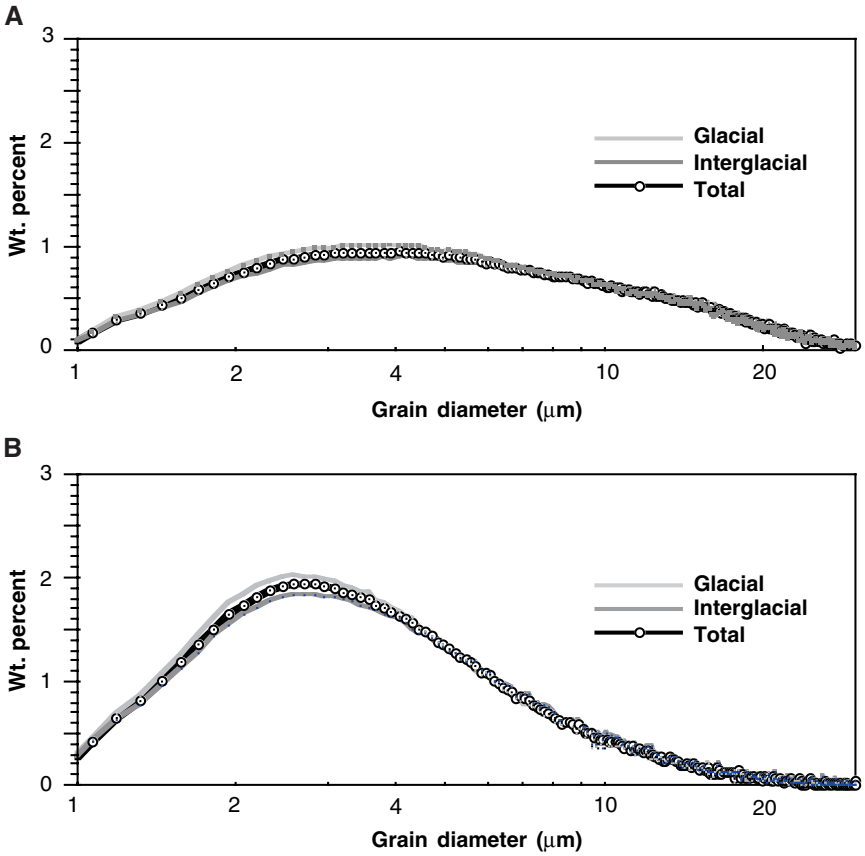

Figure 5. Average grain-size distribution of terrigenous sediment at (**A**) Site 1018 and (**B**) Site 1020.

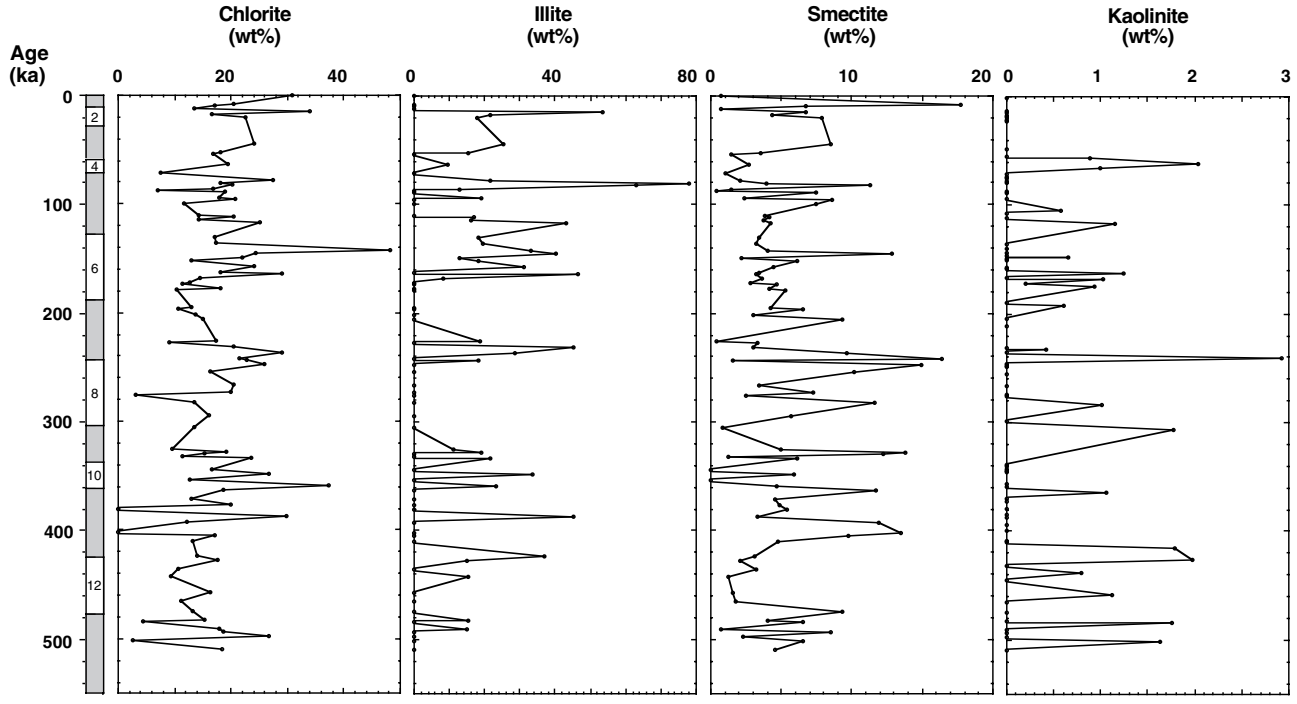

Figure 6. Clay mineral abundance for the <2-μm fraction of terrigenous material deposited at Site 1020.

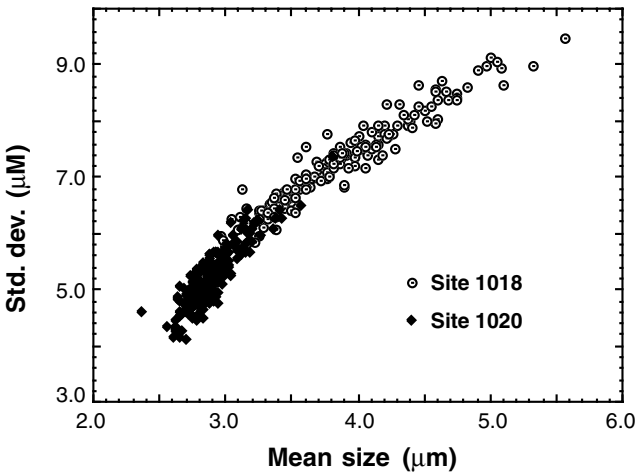

Figure 7. Grain-size data for both sites plotted together. Sediments from Site 1020 may represent a distal counterpart to sediments from Site 1018.

This has important implications in our interpretation of the terrigenous flux records. If lower sea level during glacial episodes caused increased terrigenous mineral flux at both sites during these times, then grain-size data should also show similar temporal patterns. But records of terrigenous grain size contain much higher frequency variability than terrigenous accumulation rate data and display no obvious Milankovitch periodicity (Figs. 2, 3). Thus, it seems likely that increased terrigenous input during glacial times reflects enhanced supply from the continental source region. These findings are consistent last glacial maximum climate reconstructions made from vegetational history and lake-level records in the southwestern United States (Van Devender et al., 1987; Mifflin and Wheat, 1979) but contrast with those from the Northwest (Barnosky et al., 1987).

Perhaps just as significant is the remarkable similarity observed between grain-size distributions throughout glacial cycles of the late Pleistocene (Fig. 5). Glacial size distributions are nearly identical to interglacial size distribution within sediments examined at each site and give no indication of changes in the energy of transport or type of depositional processes associated with sea level or other glacial–interglacial variability.

CONCLUSIONS

1. The terrigenous component at Sites 1018 and 1020 is dominated by hemipelagic transport and drift depositional processes throughout the late Pleistocene. Terrigenous mass flux records are closely linked to orbital-scale variability and show increased input during times of increased $\delta^{18}O$ (glacial), indicating increased supply from the source region that may be associated with increased erosional supply, either from greater exposure of shelf regions during lower sea levels, increased fluvial discharge from wetter regional source areas during these intervals, or a combination of both.
2. Detailed grain-size analysis can help distinguish the relative contribution of different terrigenous mineral transport/depositional processes and suggests that higher energy regimes were associated with sediment deposits at Site 1018, whereas Site 1020 sediments were dominated by lower energy hemipelagic processes. Average grain-size distributions within each site are nearly identical during glacial and interglacial intervals, indicating little difference between the energy of transport and depositional processes at those times.
3. Clay mineralogy patterns suggest that periods of increased terrigenous input can be explained by transport of materials primarily from source regions similar to Central and Northern California.

ACKNOWLEDGMENTS

I am deeply indebted to Dr. Dave Rea for his support during this project, particularly the generous access to his laboratory and Coulter Counter equipment and especially his moral and scientific guidance. Steve Clemens and Eve Arnold were very helpful in their reviews of this manuscript, and their insight was greatly appreciated. This work was supported by funding provided by USSSP, an Indiana University of Pennsylvania Senate grant, and a National Science Foundation summer internship program for undergraduates.

REFERENCES

Barnosky, C.W., Anderson, P.M., and Bartlein, P.J., 1987. The northwestern U.S. during deglaciation: vegetational history and paleoclimatic implications. *In* Ruddiman, W.F., and Wright, H.E., Jr. (Eds.), *North America and Adjacent Oceans During the Last Deglaciation.* Geol. Soc. Am., Geol. of North Am. Ser., K-3:289–321.

Biscaye, P.E., 1965. Mineralogy and sedimentation of recent deep-sea clays in the Atlantic Ocean and adjacent seas and oceans. *Geol. Soc. Am. Bull.,* 76:803–832.

Boven, K.L., and Rea, D.K., 1998. Partitioning of hemipelagic and eolian sedimentation in Eastern Pacific core TR163-31B. *J. Sediment. Res.,* 68:850–855.

Boyce, R.E., 1976. Definitions and laboratory techniques of compressional sound velocity parameters and wet-water content, wet-bulk density, and porosity parameters by gravimetric and gamma-ray attenuation techniques. *In* Schlanger, S.O., Jackson, E.D., et al., *Init. Repts. DSDP,* 33: Washington (U.S. Govt. Printing Office), 931–958.

Dowling, L.M., and McCave, I., N., 1993. Sedimentation on the Fenni Drift and late Glacial bottom water production in the northern Rockall Trough. *Sediment. Geol.*,82:79–87.

Ellwood, B.B., and Ledbetter, M.T., 1977. Antarctic bottom water fluctuations in the Vema Channel: effects of velocity changes on particle alignment and size. *Earth Planet. Sci. Lett.,* 35:189–198.

————, 1979. Paleocurrent indicators in deep sea sediment. *Science,* 203:837–839.

Griggs, G.B., 1987. The productions, transport and delivery of coarse-grained sediment by California coastal streams. *Coastal Sediments,* 1825–1838.

Griggs, G.B., and Hein, J.R., 1980. Sources, dispersal and clay mineral composition of fine-grained sediment off central and northern California. *J. Geol.,* 88:541–566.

Heath, G.R., and Pisias, N.G., 1979. A method for the quantitative estimation of clay minerals in North Pacific deep-sea sediments. *Clays Clay Miner.,* 27:175–184.

Imbrie, J., Hays, J.D., Martinson, D.G., McIntyre, A., Mix, A.C., Morley, J.J., Pisias, N.G., Prell, W.L., and Shackleton, N.J., 1984. The orbital theory of Pleistocene climate: support from a revised chronology of the marine $\delta^{18}O$ record. *In* Berger, A., Imbrie, J., Hays, J., Kukla, G., and Saltzman, B. (Eds.), *Milankovitch and Climate* (Pt. 1), NATO ASI Ser. C, Math Phys. Sci., 126:269–305.

Joseph, L.H., Rea, D.K., and van der Pluijm, B.A., 1998. Use of grain-size and magnetic fabric analyses to distinguish among depositional environments. *Paleoceanography,* 13:291–501.

Karlin, R., 1980. Sediment sources and clay mineral distributions off the Oregon coast. *J. Sediment. Petrol.,* 50:543–560.

Krissek, L.A., 1982. Sources, dispersal, and contributions of fine-grained terrigenous sediments on the Oregon and Washington continental slope [Ph.D. dissert.]. Oregon State Univ., Corvallis.

Ledbetter, M.T., 1986. Bottom-current pathways in the Argentine Basin revealed by mean silt particle size. *Nature,* 321:423–425.

Lyle, M., Koizumi, I., Richter, C., et al., 1997. *Proc. ODP, Init. Repts.,* 167: College Station, TX (Ocean Drilling Program).

Mifflin, M.D., and Wheat, M.M., 1979. Pluvial lakes and estimated pluvial climates of Nevada. *Nev. Bur. Mines Geol. Bull.,* 94.

Milliman, J.D., and Syvitski, J.P.M., 1992. Geomorphic/tectonic control of sediment discharge to the ocean: the importance of small mountainous rivers. *J. Geol.,* 100:525–544.

Petschick, R., Kuhn, G., and Gingele, F., 1996. Clay mineral distribution in surface sediments of the South Atlantic: sources, transport, and relation to oceanography. *Mar. Geol.,* 130:203–229.

Rea, D.K., 1992. Delivery of Himalayan sediment to the northern Indian Ocean and its relation to global climate, sea level, uplift, and seawater strontium. *In* Duncan, R.A., Rea, D.K., Kidd, R.B., von Rad, U., and Weissel, J.K. (Eds.), *Synthesis of Results from Scientific Drilling in the Indian Ocean.* Geophys. Monogr., Am. Geophys. Union, 70:387–402.

Rea, D.K., and Hovan, S.A., 1995. Grain-size distribution and depositional processes of the mineral component of abyssal sediments: lessons from the North Pacific. *Paleoceanography,* 10:251–258.

Rea, D.K., and Janecek, T.R., 1981. Mass-accumulation rates of the non-authigenic inorganic crystalline (Eolian) component of deep-sea sediments from the western mid-Pacific Mountains, Deep Sea Drilling Project Site 463. *In* Theide, J., Vallier, T.L., et al., *Init. Repts. DSDP,* 62: Washington (U.S. Govt. Printing Office), 653–659.

Shipboard Scientific Party, 1997a. Site 1018. *In* Lyle, M., Koizumi, I., Richter, C., et al., *Proc. ODP, Init. Repts.,*167: College Station, TX (Ocean Drilling Program), 311–352.

————, 1997b. Site 1020. *In* Lyle, M., Koizumi, I., Richter, C., et al., *Proc. ODP, Init. Repts.,*167: College Station, TX (Ocean Drilling Program), 389–429.

Van Devender, T.R., Thompson, R.S., and Betancourt, J.L., 1987. Vegetation history of the deserts of southwestern North America: the nature and timing of the Late Wisconsin-Holocene transition. *In* Ruddiman, W.F., and Wright, H.E., Jr. (Eds.), *North American and Adjacent Oceans During the Last Deglaciation:* Boulder, CO (Geol. Soc. Am.), 323–352.

Date of initial receipt: 15 October 1998
Date of acceptance: 25 August 1999
Ms 167SR-207